Case Studies in Thermal Engineering 63 (2024) 105388

Contents lists available at ScienceDirect

Case Studies in Thermal Engineering

journal homepage: www.elsevier.com/locate/csite

Energy and exergy analysis of a newly designed photovoltaic thermal system featuring ribs, petal array, and coiled twisted tapes: Experimental analysis

Banw Omer Ahmed [a], Adnan Ibrahim [a,*], Hariam Luqman Azeez [a], Sharul Sham Dol [b,**], Ali H.A. Al-Waeli [c], Mahmoud Jaber [a]

[a] Solar Energy Research Institute, Universiti Kebangsaan Malaysia, 43600, Bangi, Selangor, Malaysia
[b] Department of Mechanical and Industrial Engineering, Abu Dhabi University, Abu Dhabi, PO Box 59911, United Arab Emirates
[c] Engineering Department, American University of Iraq, Sulaimani, Kurdistan Region, Sulaimani, Iraq

ARTICLE INFO

Keywords:
Ribs and petal arrays
Coiled twisted tapes
SiC enhanced nanofluid and NPCM
PVT system

ABSTRACT

Photovoltaic systems suffer from electrical efficiency loss due to increases in surface temperature. To tackle this problem, Photovoltaic Thermal, consisting of photovoltaic and tube configurations attached to its back, is suggested. This study attempts to develop a new collector design in photovoltaic thermal systems. The new design features ribs and petal arrays on its inner and outer surfaces and a coiled twisted tape positioned inside it. The study also uses silicon carbide enhanced nanofluid (0.3 % and 6 % volume concentration) and phased changing material (1 % volume concentration) to boost the thermal efficiency further. Using an indoor solar simulator, the study investigates the effects of mass flow rate in the range of (0.1–0.85) kg/s, solar irradiances of (400–1000) W/m^2, and coolant types of (water, 0.3 % and 0.6 % SiC enhanced nanofluid, water and nanophase changing materials, and 0.3 % and 0.6 % SiC enhanced nanofluid and nanophase changing materials). Besides revealing the relationship between all the parameters studied, the results report a maximum electrical energy efficiency of 11.2 %, thermal energy efficiency of 86.2 %, and total exergy efficiency of 15.3 %. The system reached optimal power production of 25.99 W using a photovoltaic module with a maximum power rate of 30 W.

1. Introduction

Recently, there has been a significant surge in demand for the adoption of solar technology, especially photovoltaic (PV) [1]. This can be attributed to several factors, such as its environmentally friendly nature, cost-effectiveness, and flexibility in installation and maintenance [2]. Considering all the myriad benefits PV offers in conjunction with the concerted global push by scientific communities, governments, and international organizations against traditional sources of energy production, especially fossil fuels, PV has become one of the potential choices of the future [3]. Nevertheless, research has reported that PV is fundamentally prone to losing efficiency due to temperature rise in its surface area [4]. It has been confirmed that every 1 °C rises in the surface area of a PV results in a 0.5 % corresponding loss in electrical efficiency [5]. This issue is certainly of grave concern, given the amount of loss produced

* Corresponding author.
** Corresponding author.
E-mail address: iadnan@ukm.edu.my (A. Ibrahim).

https://doi.org/10.1016/j.csite.2024.105388
Received 17 May 2024; Received in revised form 18 September 2024; Accepted 28 October 2024
Available online 30 October 2024

rapidly increases as more solar irradiances are applied [6].

Therefore, scientists have explored many options to mitigate this problem. One of the most recognized approaches to substantially eliminate this problem is to design a Photovoltaic Thermal system (PVT), which involves the circulation of fluid behind the back of the PV to cool down the surface temperature of the PV [7]. Over the last four decades, PVT has been given particular emphasis, especially regarding enhancing its thermal and electrical efficiencies [8]. Various techniques have been employed to maximize the overall performance of PVT systems. However, passive cooling techniques have emerged as one of the most preferred methods by which PVT's efficiency has been boosted [9]. These techniques exploit natural principles without any need for external force or energy utilization, relying alternatively on increasing the contacting area, modifying microstructure, improving surface conditions, disturbing boundary layers, inducing the creation of vortex, creating more turbulence in the flow, etc. [10,11]. The application of nanofluid (NF), nano-phase changing material (NPCM), ribs, and coiled twisted tape are common practices in PVT systems [12].

Since water has low thermophysical properties, researchers have employed NF to cool down the surface temperature of PV. NFs are fluids with nanoparticles (usually metals or mental oxide) integrated into their structures which help in enhancing the fluid's thermophysical properties such as density, viscosity, and thermal conductivity [13]. For instance, Jabeen et al. [14] have used SiC enhanced NF in their new design of PVT and obtained optimal thermal and electrical efficiency of 45.13 % and 15.37 %, respectively. In another study, Büyükalaca et al. [15] employed hexagonal boron nitride enhanced NF to their PVT collector. Using IA techniques, they have developed a model which demonstrates the superior performance of the NF collector over the water based one. Lastly, Al-Aasam et al. [16] have also employed SiC enhanced NF, and their result demonstrates that electrical and thermal efficiency of 9.46 % and 88.3 % have been obtained, respectively.

Another powerful technique that is found in the literature is employing PCM. (PCM) are substances that absorb or release significant amounts of heat during phase transitions. More recent literature has introduced NPCM (PCM with nanoparticles usually metal or metal oxide) which demonstrates better thermophysical properties, making it more suitable for the application of PVT systems. Bassam et al. [17] have used SiC enhanced PCM with 1 % volume concentration in their new design of PVT, and their findings have indicated that the impact of the NPCM has been significant to the extent that electrical and thermal energy efficiency reached 10.8 % and 83.3 % respectively. Similarly, Aziz et al. [18] reported that their design of PVT, which employs NPCM, resulted in an electrical energy efficiency of 10 % and a thermal energy efficiency of 86.5 %. Finally, Maseer et al. [19] used aluminium oxide enhanced PCM and recorded a 14.04 % improvement in overall efficiency compared to the case of using bare PV.

In addition to NF and NPCM, the profile design of the absorber tube also impacts the system's thermal performance. Heat transfer enhancement will be obtained as the absorber tube's surface condition increases. Literature has offered many ways to improve the surface conditions of absorber tubes, such as incorporating ribs, dimples, fins, etc. [20]. A powerful technique to enhance heat transfer is to employ ribs in the tube design [21]. Usually, ribs are extended surfaces applied to a tube to increase heat transfer by increasing area and changing the flow condition. Aljibory et al. [22] have investigated the effects of annular ribs on heat transfer enhancement. It has been confirmed that the heat transfer coefficient is increased by 84.3 %. Moreover, Li et al. [23] increased the heat transfer coefficient by 120 % using discreet double inclined rib. Finally, Hasan et al. [24] have studied the effects of ribs on friction and entropy generation, which are the main drawbacks of passive cooling techniques in general. Their findings demonstrated that friction and entropy generation can be minimized in the application of ribs by optimizing the design parameters of the absorber tube.

Additionally, inserting twisted tapes and coils in a tube will enhance heat transfer by increasing contact area and creation of vortices [25]. Ard et al. [26] have employed a clockwise and counterclockwise twisted tape to a tube, and their contribution yielded about a 90 % increase in Nusselt number compared to a smooth tube. Similarly, Bass et al. [27] investigated the Reynold number range over which twisted tapes work best, and their results showed that they work best when the Reynold number is low. Additionally, Promvonge et al. [28] have compared the effects of a twisted tape alone and a coiled twisted tape on the thermal performance of an absorber tube. Their results have indicated that a coiled twisted tape enhances the thermal performance of the absorber twice as much as a stand-alone twisted tape.

Nomenclature

A_{PV}	Area of the solar panel (m^2)	T_{in}	Temperature of fluid in the inlet of the pipe (°C)
CP	Specific heat (J/kg K)	T_{out}	Temperature of fluid in the outlet of the pipe (°C)
$\dot{E}_{in}$	Energy in (W)	T_s	Sun temperature (°C)
$\dot{E}_{el}$	Electrical energy (W)	T_a	Ambient temperature (°C)
$\dot{E}_{mass\ in}$	Energy due to inlet flow (W)	V_{oc}	Voltage of open circuit (V)
$\dot{E}_{mass\ out}$	Energy due to outlet flow (W)	Vmax	Maximum voltage (V)
$\dot{E}_{th}$	Thermal energy (W)	u	Velocity (m/s)
$\dot{E}_{loss}$	Energy loss (W)	**The Greek symbols**	
$\dot{E}_{out}$	Energy out (W)	$\varnothing$	Nanoparticle volume fraction %
$\dot{E}_{sun}$	Sun energy (W)	ρ_{nb}	Nanofluid density (kg/m^3)
$\dot{E}_p$	Energy pump (W)	ρ_{bf}	Density of based fluid (kg/m^3)
$\dot{E}X_{in}$	Exergy in (W)	ρ_{nb}	Density of nanoparticles (kg/m^3)
$\dot{E}X_{el}$	Electrical exergy (W)	ρ_{nf}	Density of nanofluid (kg/m^3)
$\dot{E}X_{mass\ in}$	Exergy due to inlet flow (W)	ρ_{np}	Density of nanoparticle (kg/m^3)
$\dot{E}X_{mass\ out}$	Exergy due to outlet flow (W)	μ_{bf}	Viscosity of based fluid (Pa. s)
$\dot{E}X_{loss}$	Exergy loss (W)	μ_{nf}	Viscosity of nanofluid (Pa. s)
$\dot{E}X_{sun}$	Sun exergy (W)	λ	Thermal conductivity (W/M. K)

(continued on next page)

(*continued*)

Nomenclature			
$\dot{E}X_{out}$	Exergy out (W)	$\dot{m}$	Mass flow rate (kg/s)
$\dot{E}X_p$	Exergy pump (W)	ρ	Density (kg/m^3)
$\dot{E}X_{th}$	Thermal exergy (W)	μ	Dynamic viscosity (Pa. s)
FF	Fill factor	τ_{gl}	Transmissivity of the glass
I_{sc}	Current of short circuit (A)	η_p	Pump efficiency (%)
I	Solar irradiance (W/m^2)	α_{cell}	The absorptivity of cell
I_{max}	Maximum current (A)	ΔP	Pressure drops (pascal)
K_{np}	Thermal conductivity of nanoparticle (W/M. K)	ε_e	Electrical exergy efficiency (%)
K_{bf}	Thermal conductivity of based fluid (W/M. K)	η_{ttotal}	Total energy efficiency (%)
K_{nf}	Thermal conductivity of nanofluid (W/M. K)	ε_{th}	Thermal exergy efficiency (%)
N	Avogadro number	ε_{total}	Total exergy (%)
P_{Max}	Maximum Power (W)	η_t	Total energy (%)
Q_u	Heat obtained (W)	η_t	Thermal efficiency (%)
		η_{el}	Electrical efficiency (%)
		ε_{total}	Total exergy (%)

Table 1
The specification of the SW30M − 36 PV module used in the experiment [29].

Model Type			SW30M-36	
Solar Cell Type			Mono	
P_{max}	V_{max}	I_{max}	V_{oc}	I_{sc}
30 W	18.9 V	1.89 A	22.9 V	1.99 A
Size Of the Panel			360 × 670 × 17 mm	
Weight			2.4 kg	
Standard Test Condition			1000 W/m^2, 1.5AM, 25 °C	
Output Tolerance			7 W	

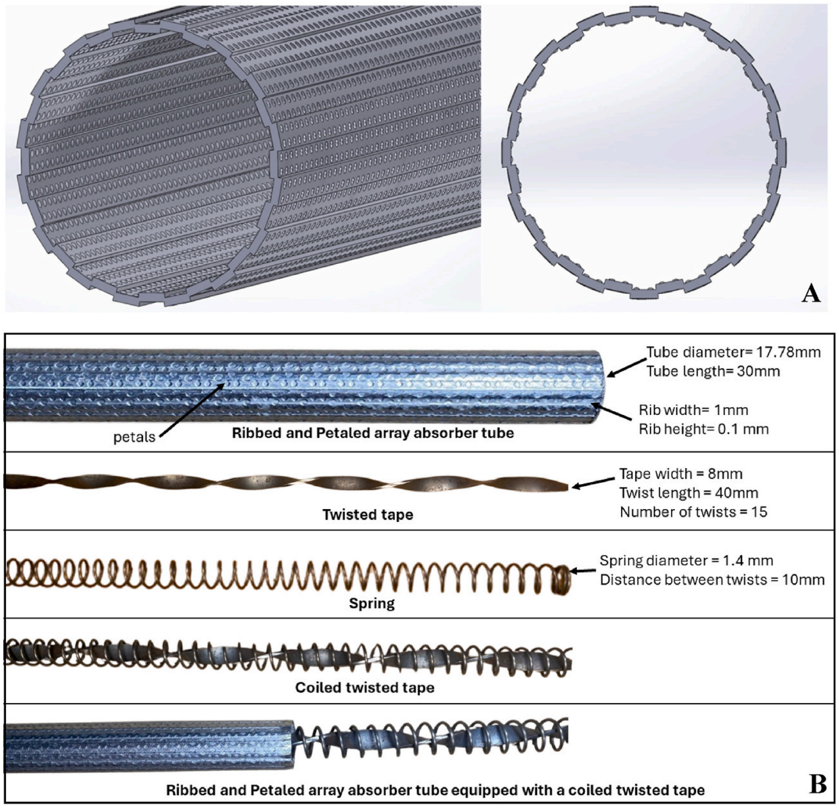

Fig. 1. A) a SolidWorks module and B) real picture and geometrical specification of the tube used in this study.

Table 2
The details of the SiC nanoparticles used in this study [17].

Manufacturer	Appearance	Purity	PH value	Crystal type	Melting point	Grain size	Thermal Conductivity	Bulk Density	Zeta potential
US Res. Nanomaterials	Greyish white	99+%	3-7 at 20 °C	Cubic	2745 °C	40–60 nm	370–490 W/m K	3.22 g/cm3	27.8 mV

Table 3
The details of the paraffin wax used in this experiment [29].

Melting point temperature	Liquid state density	Solid state density	Thermal conductivity	Solid state-specific heat	Liquid state-specific heat
49 °C	835 (kg/m^3)	935 (kg/m^3)	0.23 (W/m°C)	2100 (J/kg °C)	2100 (J/kg °C)

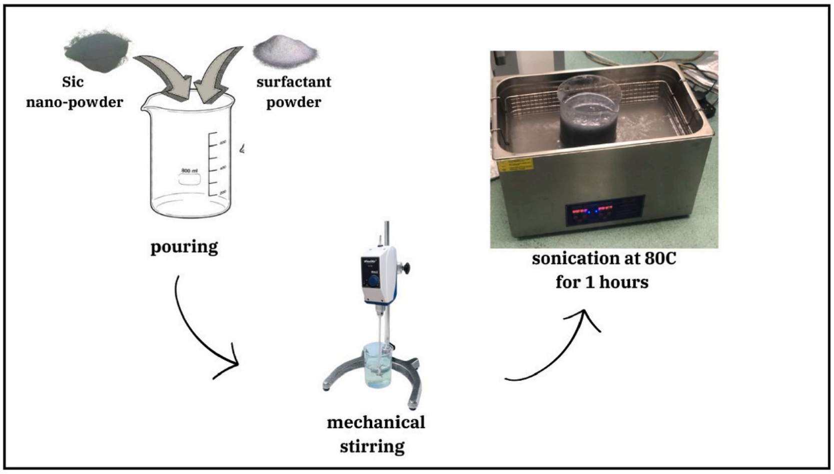

(A)

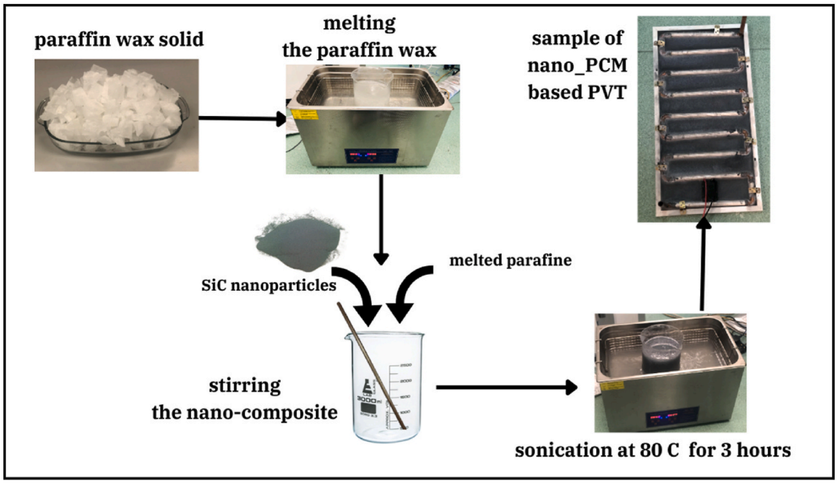

(B)

Fig. 2. Step-by-step preparation of A) NF and B) NPCM.

Despite all the improvements documented in the literature, there is still a significant gap regarding developing a collector design which shows outstanding thermal performance. The two latest design of Bassam et al. [17] and Al-Aasam [16] are evidence of the gap since they only achieved maximum power of 20 W using a 30 W P module.

- Having stated the research gap to which this study is devoted, the new collector design is suggested, which features ribs, petals arrays, and a coiled twisted tape. It additionally uses 0.3 % and 0.6 % SiC enhanced NF and 1 % SiC enhanced PCM.

The main application of this study is to help countries with hot climates incorporate PV technology into their energy infrastructure more efficiently. The PVT study was conducted indoor encompassing mass flow rates of (0.1, 0.025, 0.4, 0.55, 0.7, 0.85) kg/s, solar irradiance of (400, 600, 800, and 1000) W/m^2, and coolant types of (water, 0.3 % and 0.6 % SiC enhanced nanofluid, water and nanophase changing materials, and 0.3 % and 0.6 % SiC enhanced nanofluid and nanophase changing materials). The output of the study is a meticulous investigation of energy, exergy, and power production of the studied PVT systems. The selected mass flow rates, solar irradiances, and coolant types are chosen for reasons such as they are the best range over which performance is enhanced, match real-world applications, and technical and economically are feasible.

2. Methodology

2.1. Physical model

PVT consists of two main parts namely, PV and a thermal collector in a form of tube configurations. This study uses a mono-crystalline PV module called SW30M − 36 with the specifications outlined in Table 1. Literature has shown that nine lines of pipe in a serpentine configuration optimizes heat transfer in the case of a PV with an area of 0.24 m^2 [17]. As mentioned, the study utilizes a special pipe featuring ribs and petal arrays designed on its inner and outer surface to enhance heat transfer. Also, the study placed a coiled twisted tape made from carbon steel in the tube to increase thermal performance by increasing the contact area further, creating more turbulence in the flow and inducing the formation of a vortex. Fig. 1 provides a pictorial demonstration and geometrical specification of the newly designed collector.

2.2. Nanofluid and nanophase changing material preparation procedures

Before conducting the experiment, the NF and NPCM must be prepared. The study will prepare two volume concentration of SiC enhanced NF namely 0.3 % and 0.6 %. It will also prepare 1 % SiC enhanced PCM. Regarding the NF preparation, for every 24 litters of water, 463.2 g of SiC nanoparticles will be used for 0.6 % volume concentration and 231.6 g of SiC nanoparticles for 0.3 % volume concentration [29]. Nevertheless, in the case of the NPCM, for every 2.5 kg of melted paraffin wax, 100 g of SiC nanoparticles will be used to prepare 1 % volume concentration of SiC enhanced PCM [29]. Tables 2 and 3 show the details of the SiC nanoparticles and the paraffin wax used in this study.

Having scaled all the component correctly and given that water and SiC nanoparticles do not mix naturally, the study used polyvinylpyrrolidone in the NF preparation procedure. Water, surfactant of polyvinylpyrrolidone, and nanoparticle of SiC are mixed in a container and agitated for 5 min using a mechanical mixing device. Then, it will be placed in an ultrasonic bath for 3 h under the temperature of 80 °C and a vibration frequency of 50 Hz [29]. Fig. 2 (a) shows a step-by-step explanation of how to prepare the NF. Regarding NPCM preparation, paraffin wax is melted in an ultrasonic bath and mixed with SiC nanoparticles and a surfactant of polyvinylpyrrolidone. After mixing them for 5 min with a mechanical device, they will remain in an ultrasonic bath for 3 h under a temperature of 80 °C and vibration frequency of 50 Hz to guarantee homogeneity in mixing [29]. Fig. 2 (b) shows the step-by-step preparations of the NPCM.

After the NF and the NPCM are completely prepared, either their thermophysical properties or the homogeneity of their distribution must be checked to ensure that they have been prepared correctly and will have good impacts as cooling mediums.

Utilizing a device called The Anton Paar model DMA 1001 Density, the density of the NF and NPCM were figured out over a temperature range of 15–50 °C. Subsequently, the obtained result was numerically confirmed using Equation (1), [30].

$$\rho_{nf} = (1-\phi)\rho_{bf} + \phi\rho_{np} \tag{1}$$

ρ_{nf} is the density of the new mixture, ϕ is the volume percentage of each element, and ρ_{np} and ρ_{bf} are the densities of the nanoparticle and water, respectively.

The same method was applied to find the samples' viscosity and thermal conductivity, except that Anton Paar's model MCR 92 viscometer and Linseis's model THB-500 devices were employed to find the samples' viscosity and thermal conductivity, respectively, over the determined temperature range. Equations (2)–(4) also numerically confirmed the obtained results [31].

$$\mu_{nf} = \mu_{bf} \times \frac{1}{\left(1 - 3.87\left(\frac{\rho_{np}}{\rho_{bf}}\right)^{-0.3} \times \phi^{1.03}\right.} \tag{2}$$

$$\rho_{nf} = \frac{6M}{N \times \pi \times \rho_{nb}} \tag{3}$$

Where μ_{nf} and μ_{bf} are the viscosity of the NF and water, ρ_{np} and ρ_{bf} are densities of nanoparticles and density of water, M is fluid molecular weight, N is Avogadro number, and ρ_{nb} is the density of the based fluid.

Table 4
The thermophysical properties of the nanofluid.

Temp (°C)	Water			0.3%SiC			0.6%SiC		
	ρ kg/m^3	μ Pa. s	K W/M. K	ρ kg/m^3	μ Pa. s	K W/M. K	ρ kg/m^3	μ Pa. s	K W/M. K
15	999.1	1.11	0.55	1006.6	1.38	0.61	1013.3	1.47	0.63
20	998.3	1.13	0.58	1006.2	1.36	0.63	1012.9	1.47	0.66
25	997.1	1.08	0.60	1005.1	1.29	0.65	1011.9	1.39	0.68
30	995.8	0.99	0.62	1003.1	1.19	0.67	1010.5	1.27	0.69
35	994.2	0.89	0.64	1001.4	1.11	0.69	1008.9	1.18	0.71
40	992.3	0.80	0.66	999.2	1.01	0.7	1006.8	1.08	0.73
45	990.2	0.74	0.67	997.	0.97	0.71	1003.6	0.99	0.74
50	987.8	0.73	0.68	994.1	0.98	0.72	1000.6	1.01	0.75

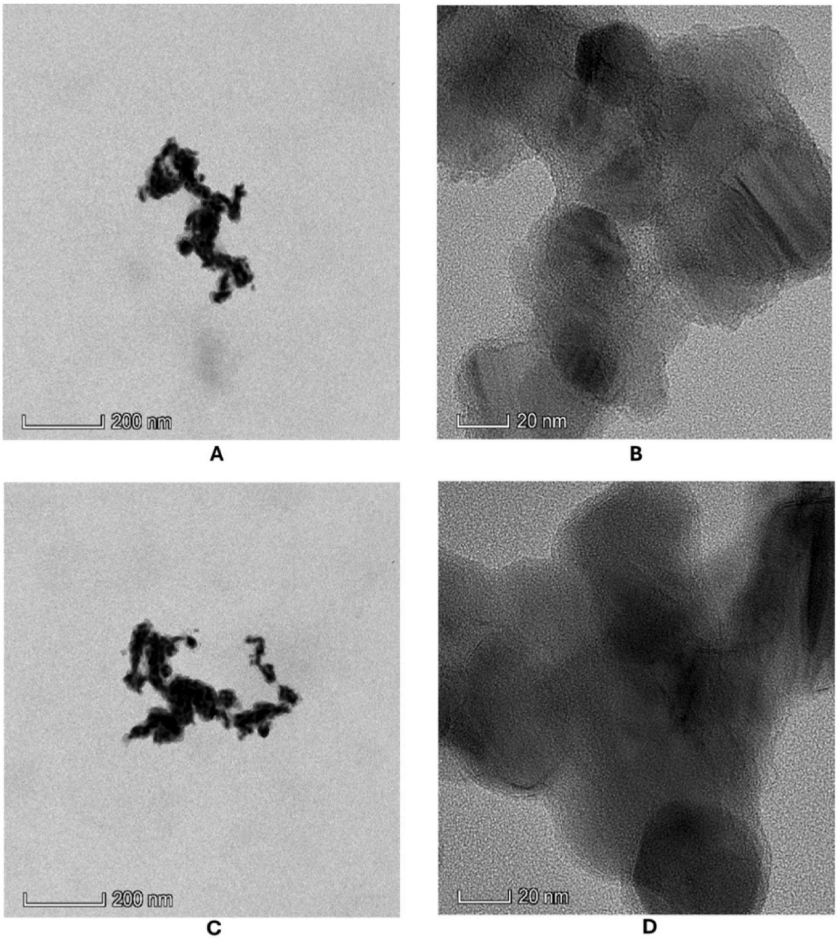

Fig. 3. TEM images of the NF and NPCM.

$$K_{nf} = \frac{K_{np} + 2K_{bf} + 2\phi(K_{np} - K_{bf})}{K_{np} + 2K_{bf} - 2\phi(K_{np} - K_{bf})} \times K_{bf} \tag{4}$$

Where K_{nf}, K_{np}, and K_{bf} are the thermal conductivity of the prepared sample, nanoparticle, and the based fluid. Finally, the specific heat capacity of the samples was numerically calculated using Equation (5) [31].

$$CP_{mix} = \frac{(1-\phi)(\rho CP)_{water} + (\phi\rho CP)_{np}}{\rho_{mix}} \tag{5}$$

Table 4 compiles the thermophysical properties of the NF over a temperature range of 15–50 °C, which is considered a good range

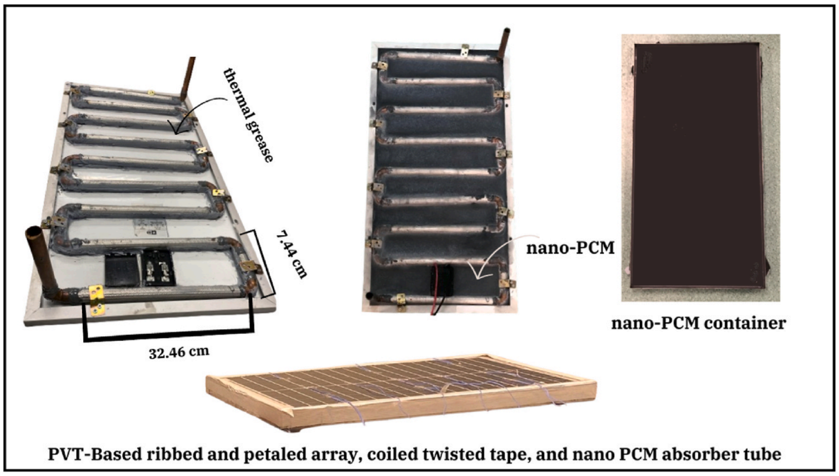

(A)

(B)

Fig. 4. A) final presentation of the PVT, B) the experimental rig, and C) the diagram of the experimental rig.

for the application of PVT. Moreover, the samples were subjected to TEM testing (Transmission Electron Microscopy) to ensure that the sample had an appropriate level of homogeneity. The image of (A and B) in Fig. 3 are the image of the NF, and (C and D) are the images of the NPCM. Both the thermophysical properties and TEM images demonstrate that the sample have improved thermophysical properties and high range of stability. The results recorded for the NF and NPCM are consistent with the literature [29].

After preparing the physical model, NF, NPCM, and nine absorber tubes made from aluminium in the serpentine configuration were attached to the back of the PV. The number of tubes and the serpentine shape are considered the best design configurations in the literature for the used module [17]. Then, the NPCM was poured on the back surface of the PV and an NPCM container. The NPCM container was manufactured to prevent the NPCM from wasting, especially when it turns into liquid at high temperatures, and it also increases the system's thermal efficiency further. Lastly, as shown in Fig. 4 (a), all the parts were collected as one module.

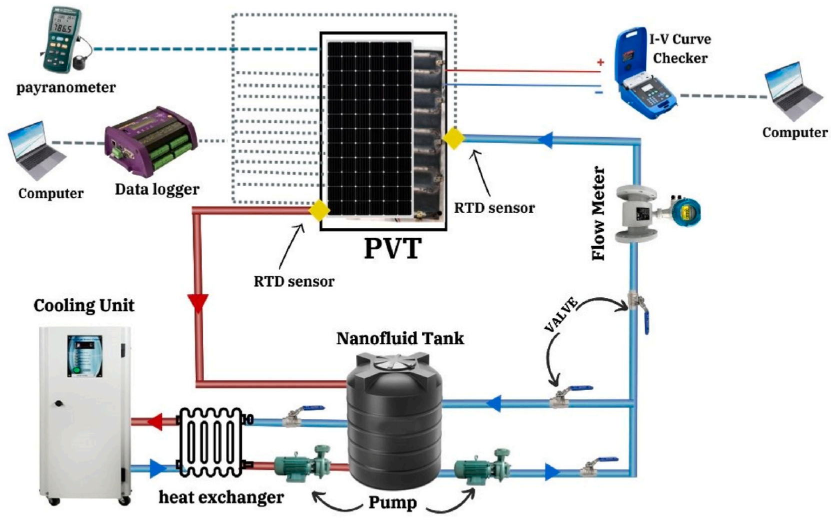

(C)

Fig. 4. (*continued*).

2.3. The experimental rig

After preparing the PVT prototype, it was integrated into the experimental setup depicted in Fig. 4(b) and (c). Fluid comes from a fluid tank; its velocity is determined through a DHYB-800 digital flow meter. Subsequently, it passes through an RTD sensor before entering the PVT to measure its temperature. Once the fluid leaves the PVT, the RTD sensor will measure its temperature again. The fluid goes back into the fluid tank, and circulation keeps repeating. A cooling unit and a heat exchanger are used to keep the temperature of the fluid tank at ambient temperature. Additionally, thermocouples are connected to the surface of the PV, and the temperature of the PV's surface is measured through a DT80 data taker. Lastly, an MP-11 I-V checker is employed to measure the electrical output of the PV. The two active component of the system are the pumps and the cooling unit. Nevertheless, all the calculation performed in this research has already subtracted the amount of energy consumed by the pumps. Moreover, in real PVT application the hot water produced will be used for other purposes, and there is no need to use a cooling unit.

2.4. The mathematical models applied in this study

The first PVT analysis that this study performs is energy balance, where the sum of the energy that enters the system, namely the energy of the sun and energy obtained due to fluid entering the system, is equal to the output energy produced, such as electrical power produced, energy form fluid leaving the system, and wastes generated in the process. Equations (6) and (7) are the energy balance equations stated mathematically [32–35].

$$\sum \dot{E}_{in} = \sum \dot{E}_{out} + \sum \dot{E}_{loss} \tag{6}$$

$$\dot{E}_{sun} + \dot{E}_{mass\ in} = \dot{E}_{el} + \dot{E}_{mass\ out} + \dot{E}_{loss} \tag{7}$$

From equation (8), the sun energy is the multiplication of the solar irradiance (I) entering the system, the area of the PV (A_{pv}), and τ_{gl} and α_{cell}, which are the transmissivity of the glass over the PV cell and the absorbability of the cells [32–35].

$$\dot{E}_{sun} = I \times A_{pv} \times \tau_{gl} \times \alpha_{cell} \tag{8}$$

The electrical output of the system can be calculated through Equations (9) and (10), where I_{sc}, V_{oc}, and FF are the current of the short circuit, the voltage of an open circuit, and the fill factor of the PV [32–35]

$$\dot{E}_{el} = I_{sc} \times V_{oc} \times FF \tag{9}$$

$$FF = \frac{I_{max} \times V_{max}}{I_{sc} \times V_{oc}} \tag{10}$$

After finding the system's electrical output and the sun's energy, the system's electrical energy efficiency can be calculated using Equation (11) [32–35].

$$\eta_e = \frac{\dot{E}_{el}}{\dot{E}_{sun}} = \frac{I_{sc} \times V_{oc} \times FF}{I \times A_{pv} \times \tau_{gl} \times \alpha_{cell}} \tag{11}$$

Equations (12) and (13) calculate the system's thermal efficiency, where all the parameters have already been explained [32–35].

$$\dot{E}_{mass\ out} - \dot{E}_{mass\ in} = \dot{E}_{th} = \dot{m} \times C_p(T_{out} - T_{in}) \tag{12}$$

$$\eta_{th} = \frac{\dot{E}_{th}}{\dot{E}_{sun}} = \frac{\dot{m} \times C_p(T_{out} - T_{in})}{I \times A_{pv} \times \tau_{gl} \times \alpha_{cell}} \tag{13}$$

The energy efficiency calculated above does not consider the amount of energy the pumps have consumed. Therefore, Equations (14)–(16) will recalculate the system's energy efficiency, considering the loss generated. In Equations (14)–(16), ρ, *and* η_p are the pressure drop, the fluid's density, and the motor's efficiency [32–35].

$$\dot{E}_{el-new} = \dot{E}_{el} - \dot{E}_p \tag{14}$$

$$\dot{E}_p = \frac{\dot{m}\ \Delta P}{\rho \eta_p} \tag{15}$$

$$\eta_{el} = \frac{\dot{E}_{el} - \dot{E}_p}{\dot{E}_{sun}} \tag{16}$$

The second analysis this study has performed is exergy analysis, where again the sum of inlet exergy, which is exergy from the sun, and exergy of the fluid entering the system is equal to the sum of exergy leaving the system, such as electrical exergy, exergy due to fluid leaving the system, and finally exergy loss. Equations (17) and (18) are a mathematical statement of the exergy balance equation [32–35].

$$\sum \dot{E}X_{in} = \sum \dot{E}X_{out} + \sum \dot{E}X_{loss} \tag{17}$$

$$\dot{E}X_{sun} + \dot{E}_{mass\ in} = \dot{E}X_{el} + \dot{E}X_{mass\ out} + \dot{E}X_{loss} \tag{18}$$

Lastly, the same process is repeated to calculate the exergy of the system with the exception that exergy equations always consider the effect of ambient temperature since, ultimately, exergy is defined by the available amount of energy of the system. Through equations (19)–(24), the total exergy produced in the system is calculated [32–35].

$$\dot{E}X_{sun} = I \times A_{pv}\left(1 - \frac{T_a}{T_s}\right) \tag{19}$$

$$\dot{E}X_{el-new} = \dot{E}X_{el} - \dot{E}X_p \tag{20}$$

$$\varepsilon_e = \frac{\dot{E}X_{el} - \dot{E}X_p}{I \times A_{pv}\left(1 - \frac{T_a}{T_s}\right)} = \frac{(I_{sc} \times V_{oc} \times FF) - \left(\frac{\dot{m}\ \Delta P}{\rho \eta_p}\right)}{I \times A_{pv}\left(1 - \frac{T_a}{T_s}\right)} \tag{21}$$

$$\dot{E}X_{mass\ out} - \dot{E}X_{mass\ in} = \dot{E}X_{th} = \dot{m} \times \left[C_p(T_{out} - T_{in}) - T_a C_p\ ln\left(\frac{T_{out}}{T_{in}}\right)\right] \tag{22}$$

$$\varepsilon_{th} = \frac{\dot{E}X_{th}}{\dot{E}X_{sun}} = \frac{\dot{m} \times \left[C_p(T_{out} - T_{in}) - T_a C_p\ ln\left(\frac{T_{out}}{T_{in}}\right)\right]}{I \times A_{pv}\left(1 - \frac{T_a}{T_s}\right)} \tag{23}$$

$$\varepsilon_{total} = \varepsilon_{th} + \varepsilon_e \tag{24}$$

2.5. Uncertainty analysis

Before performing any calculation, it should be mentioned that the devices used in this experiment have allowances for mistakes. Thus, Table 5 and Equation (25) will calculate the percentage of error in the study [36].

$$W_R = \left[\left(\frac{\partial R}{\partial X_1} W_1\right)^2 + \left(\frac{\partial R}{\partial X_2} W_2\right)^2 + \ldots \left(\frac{\partial R}{\partial X_n} W_n\right)^2\right]^{0.5} \tag{25}$$

Table 5
Error allowance for the used devices.

Equipment	Measured parameter	Uncertainty
RTD Sensor	Inlet and outlet temperature	±0.01
Thermocouple K type	Temperature	±0.1
TES pyranometer	Solar irradiance	±1.5
DHYB-800 digital flow meter	Mass flow rate	±0.5 %
DT80 data taker	Surface temperature	±0.01
MP-11 I-V checker	Voltage & Current	±1.0

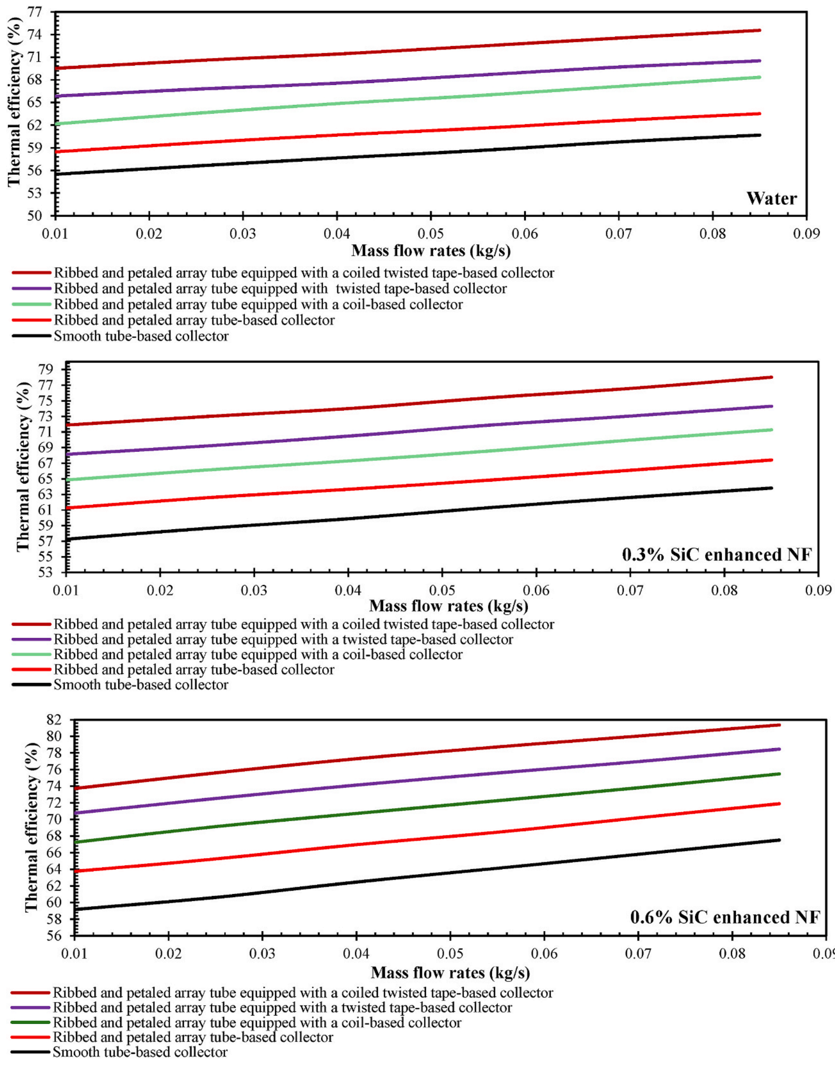

Fig. 5. (A, B, and C) are the thermal efficiencies of five collectors at solar irradiances of 1000 W/m^2.

$$W = \left[(0.01)^2 + (0.1)^2 + (1.5)^2 + (0.5)^2 + (0.01)^2 + (1)^2\right]^{0.5}$$

$$W = 1.58\%$$

3. Results and Dissuasion

3.1. Optimizing thermal energy efficiency

Prior to conducting the PVT experiment, this study aimed to elucidate the contribution of each component in the new collector

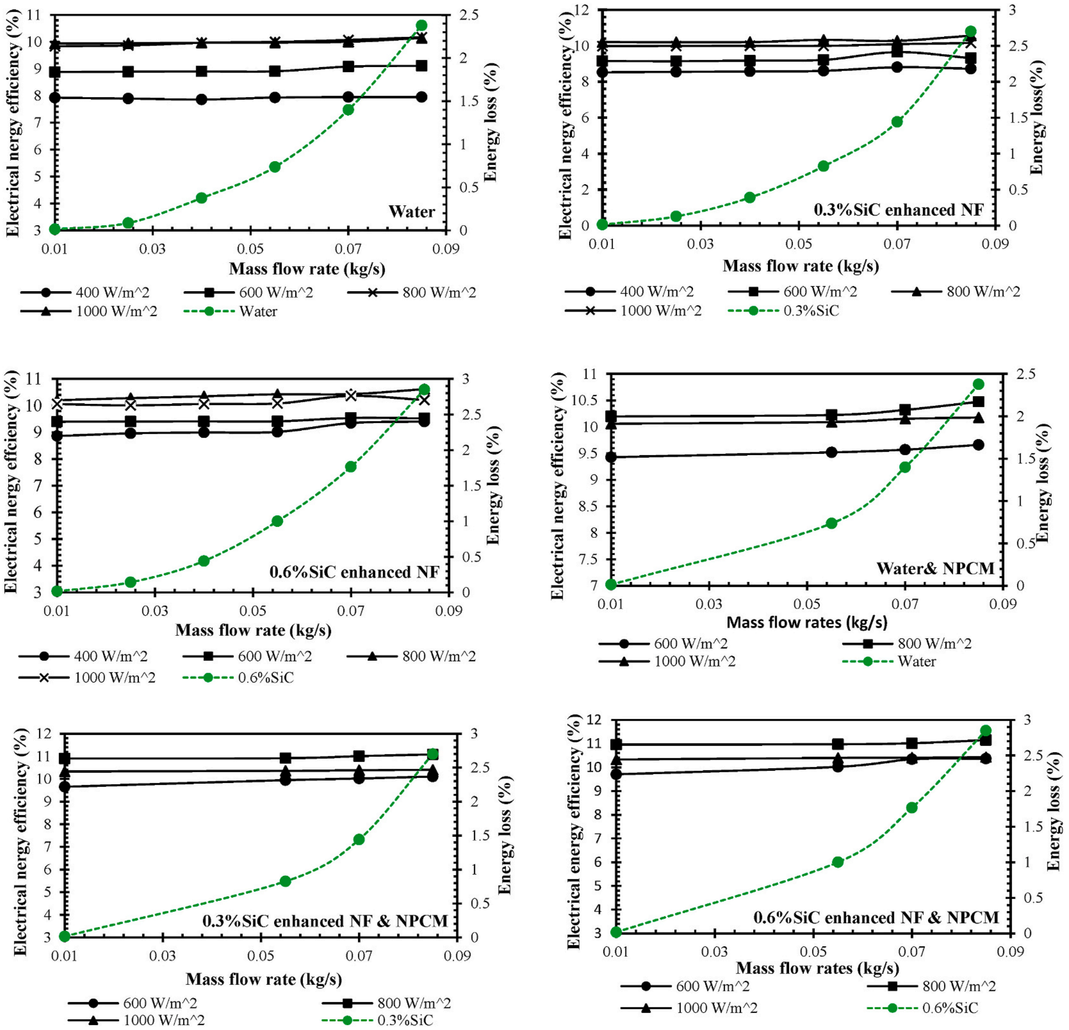

Fig. 6. The electrical energy efficiency and energy loss recorded for all the cases of this study over various mass flow rates, solar irradiances, and cooling medium.

design to thermal efficiency improvements and address concerns regarding the potential negative effects of increased pressure drop associated with additional components. Thermal efficiency analysis was assessed for five distinct collector designs varying in their base absorber tubes under a solar irradiance of 1000 W/m^2, namely: a smooth tube, a ribbed and petaled array tube, a ribbed and petaled array tube with a coil, a ribbed and petaled array tube with a twisted tape, and a ribbed and petaled array tube with both a coil and twisted tape. Data presented in Fig. 5 reveals that the new design significantly outperforms all the other designs, especially the smooth tube-based collector, showing thermal efficiency enhancements of 18.6 % with water, 22.2 % with 0.3 % SiC enhanced NF, and 25.4 % with 0.6 % SiC enhanced NF at a mass flow rate of 0.085 kg/s. These improvements are attributed to increased contact area, enhanced turbulence, and vortex formation facilitated by the new design. Despite the additional components contributing to higher pressure drops, the thermal efficiency gains achieved by the new design are sufficient to offset these drawbacks, leading to overall superior performance compared to all the other designs, and particularly the smooth tube-based collector.

3.2. Electrical energy efficiency and energy loss

The system's electrical energy efficiency demonstrates a positive correlation with mass flow rates as it is the case in the literature [37]. This is because as the fluid circulates faster, cold water meets hot surfaces sooner. Conversely, the relationship between solar irradiance and electrical energy efficiency is more ambiguous. While the energy efficiency increases for solar irradiance of 400, 600, and 800 W/m^2, it encounters a decline for solar irradiance of 1000 W/m^2 [38]. For instance, the energy efficiency of 7.95 %, 9.11 %, 10.16 %, and 10.14 % are recorded for solar irradiances of 400, 600, 800, and 1000 W/m^2 when the mass flow rate of 0.085 kg/s and water as a cooling medium is employed. This phenomenon can be attributed to the fact that as solar irradiance is low, sufficient cooling capacity is provided for the system to function well. However, as solar irradiances increase, the system's cooling capacity starts to

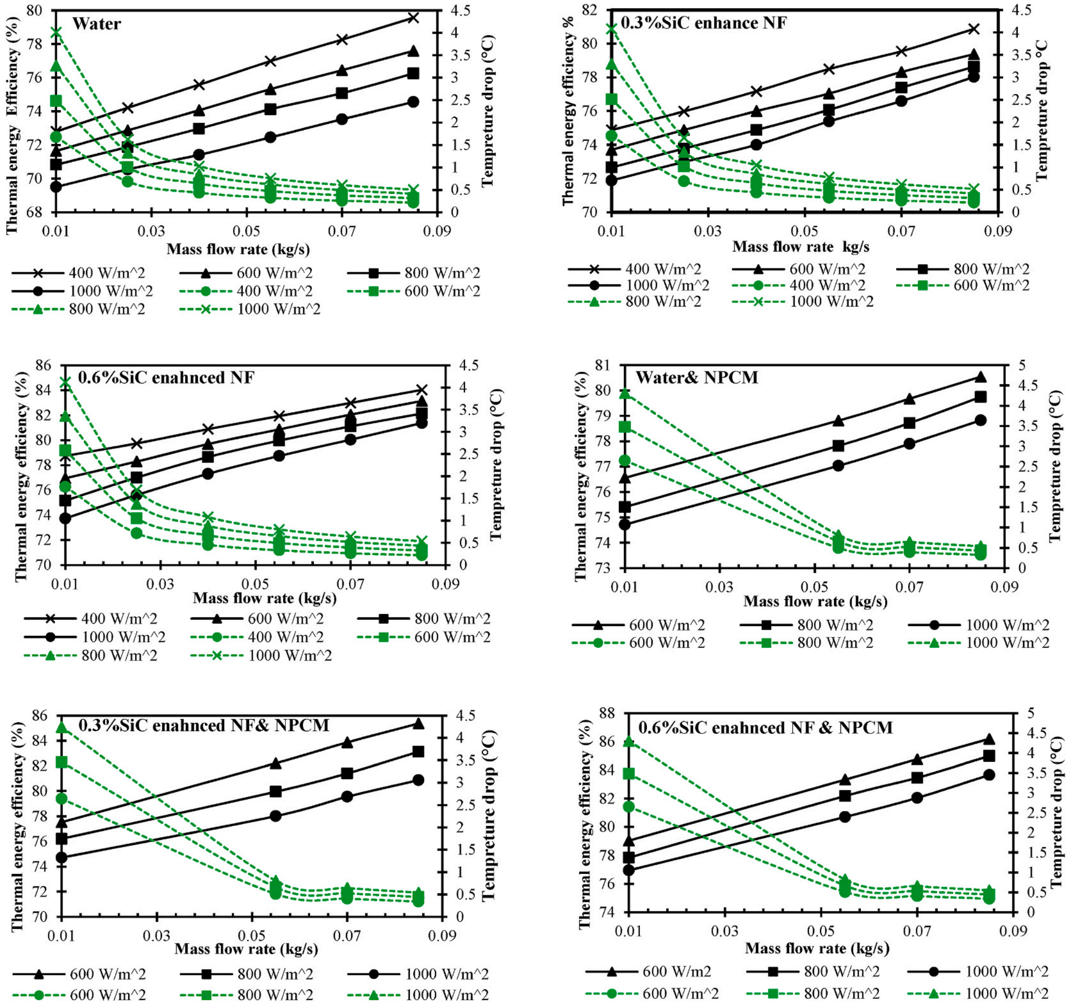

Fig. 7. Temperature differences and thermal efficiencies for all the cases of the study at various mass flow rates, cooling medium, and solar irradiances.

encounter insufficiency, resulting in a declining trend in energy efficiency. Additionally, as cooling techniques change from water to 0.3%SiC and 0.6%SiC enhanced NF, the electrical energy efficiency increases by about 10–40 % for each technique. Nevertheless, the declining trend at high solar irradiances remains even when NF is employed. This provides a reasonable justification that utilizing NPCM is necessary. In the best-case scenario of employing a mass flow rate of 0.085 kg/s, solar irradiance of 800 W/m^2, and 0.6%SiC enhanced NF, the system's electrical energy efficiency reaches 10.61 %. With the incorporation of NPCM, the system's overall energy improves further. The highest electrical energy efficiency of 11.2 % is recorded when solar irradiance of 800 W/m^2, mass flow rate of 0.085 kg/s, and 0.6%SiC enhanced NF and NPCM are employed. Even though the system's energy efficiency has increased every time a new cooling technique is employed, there is still a lack of enough cooling capacity at high solar irradiances.

Lastly, as water changes to 0.3 % and 0.6 % SiC enhanced NF, the energy consumed by the pumps installed in the system increases. The reason is that energy loss because of the pump predominately relies on pressure drop. The NF with the highest concentration of nanoparticles produces the highest pressure drop. However, there will be more loss when the mass flow rate is high since the impact of the mass flow rate is more powerful than the effects of pressure drop. The pumps' highest energy consumption is 2.86 % when 0.6 % SiC enhanced NF at mass flow rate of 0.085 kg/s is employed. Fig. 6 shows energy efficiency and losses at different mass flow rates, solar irradiances, and cooling mediums. Black lines indicate system efficiency after pump energy consumption, while green lines show the energy used by the pumps.

3.3. Thermal energy efficiency analysis

An important factor affecting the thermal efficiency of a PVT system is the difference between outlet temperature and inlet temperature. Therefore, Fig. 7 shows the temperature differences and thermal efficiency for all the cases included in this research. The black lines are thermal efficiencies for various mass flow rates, solar irradiance, and cooling techniques while the green lines are the

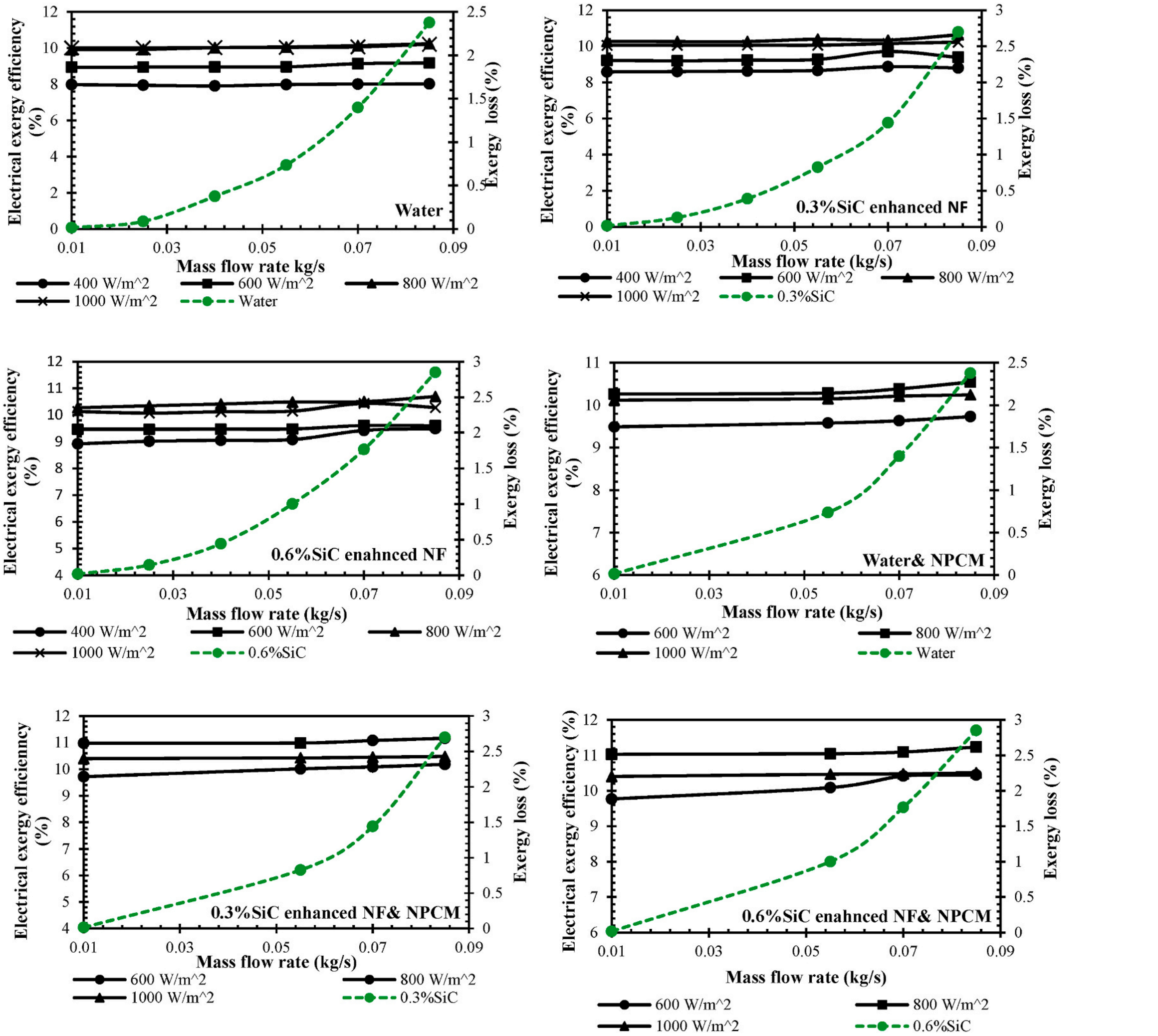

Fig. 8. The relationship between mass flow rates, electrical exergy efficiency, and the ratio of ambient temperature over the temperature of the sun over various solar irradiances and cooling medium.

temperature differences. As the mass flow rate increases from 0.01 kg/s to 0.085 kg/s, the system's thermal efficiency increases [39]. For instance, thermal efficiency of 72.5 %, 74.2 %, 75.5 %, 76.9 %, 78.2 %, and 79.5 % are recorded for mass flow rates of 0.1, 0.025, 0.4, 0.55, 0.7, and 0.85 kg/s, respectively. The trend is attributed to the fact that faster circulation of fluid provides a more effective cooling capacity. Conversely, an increase in solar irradiances exhibits a slight decline in thermal efficiency [40]. For instance, as solar irradiances increase from 400 W/m^2 to 600, 800, and 1000 W/m^2 in the cases only employing water, the thermal efficiency declines from 72.2 % to 71.6 %, 70.8 %, and 69.5 %, respectively. The reason is that more cooling capacity is needed as solar irradiances increase. Employing 0.3 % and 0.6 % of SiC enhanced NF, and NPCM increases thermal efficiency from 77.6 %, the thermal efficiency of only using water, to 79.4.6 %, 83.2 %, and 86.2 %, respectively. The temperature difference is significantly affected by the mass flow rate. In low mass flow rate ranges, the fluid stays for a long time in the PVT system, causing the outlet temperature to be significantly high. However, in fast flow rate ranges, the fluid stays for a short time in the PVT, and this causes a slight temperature rise. For instance, in the case of only employing water, the temperature difference of 1.68, 0.7, 0.4,0.3,0.25, and 0.2 °C are recorded for mass flow rates of 0.1, 0.025, 0.4, 0.55, 0.7, and 0.85 kg/s, respectively. Moreover, as solar irradiance increases, the temperature difference increases as well. Temperature differences of 1.6, 2.4, 3.2, and 4 °C are recorded for solar irradiances of 400 W/m^2 to 600, 800, and 1000 W/m^2. The reason here is that at high solar irradiances, the fluid can absorb more heat, causing a noticeable increase in the outlet temperature.

3.4. Electrical and total exergy efficiency analysis

Like electrical and thermal energy efficiency, as mass flow rate increases, electrical exergy efficiency encounters a slight increase caused by reasons delineated in the preceding discussion on electrical and thermal energy efficiency [37]. For instance, as the mass

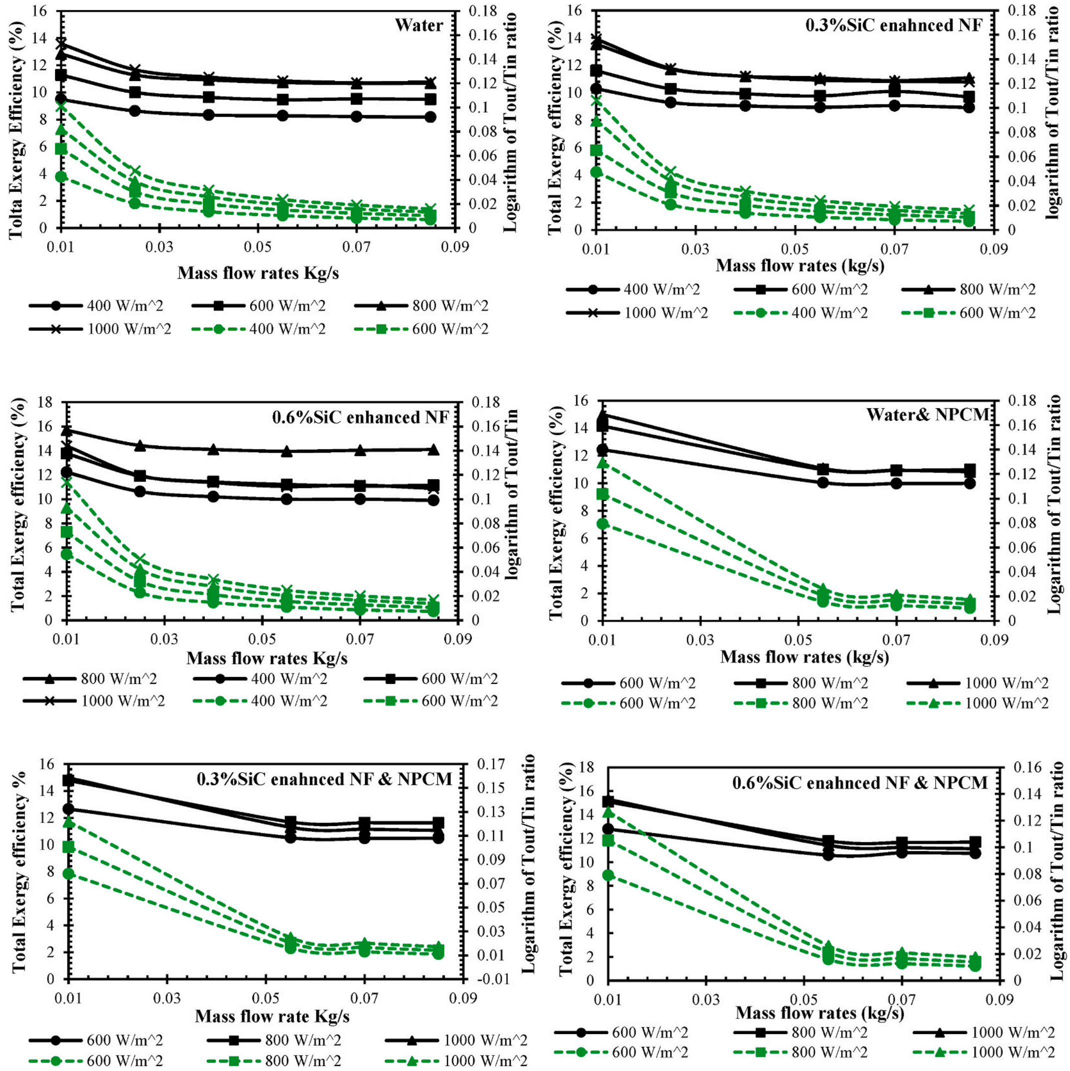

Fig. 9. The relationship between mass flow rates, total exergy, and the ratio of the logarithm of temperature differences over various solar irradiances and cooling mediums.

flow rate goes from 0.01 kg/s to 0.085 kg/s in the cases of only employing water, electrical exergy increases from 9.9 % to 10.3 %. Nevertheless, the influence of solar irradiance comes under further scrutiny. The relation is directly proportional to solar irradiances of 400, 600, and 800 W/m^2. As the solar irradiances reach 1000 W/m^2, the electrical exergy efficiency declines slightly [38]. For instance, considering the cases that only employ water, the electrical exergy efficiencies of 8.02 %, 9.2 %, 10.23 %, and 10.12 % are recorded when solar irradiances are 400, 600, 800, and 1000 W/m^2. This declining trend at high solar irradiances demonstrates that the system's cooling capacity is insufficient to maximize energy production.

Additionally, as techniques like 0.3 % SiC enhanced NF, 0.6 % SiC enhanced NF, and NPCM are employed, the electrical exergy of the system goes up from 10.23 % to 10.64 %, 10.7 %, and 11.24 % for solar irradiance of 800 W/m^2 and mass flow rate of 0.085 kg/s. Fig. 8 illustrates electrical exergy efficiency and exergy loss due to pumps for all the cases over the scope of the research. As the mass flow rate increases, so does the exergy consumed by the pumps, according to equation (15). Finally, the higher the concentration of nanoparticles in the fluid, the higher the pressure drop induced in the tube, resulting in more exergy consumed by the pumps.

Given the thermal exergy of the system does not exceed 4 %, and the total exergy already is a summation of the electrical and thermal exergy of the system, Fig. 9 shows the relations between total exergy, mass flow rate, and the logarithm of outlet temperature over inlet temperature. As the mass flow rate increases from 0.01 kg/s to 0.085 kg/s in all the cases, the total exergy of the system decreases slightly. For instance, it drops from 12.8 % to 10.6 % when the mass flow rate increases from 0.01 kg/s to 0.085 kg/s for solar irradiance of 800 W/m^2 and employing only water. The reason is that the influence of mass flow rate is more significant on thermal exergy than electrical exergy, and the relationship between mass flow rate and thermal exergy is reversely proportional. However, with increases in solar irradiance, the total exergy slowly increases for all the solar irradiances. For example, for cases employing only water,

Table 6
Comparing the finding of this study with similar cases reported in the literature.

Reference and year	Type of study	Cooling techniques	Results of the study
[17]-2023	Experimental	NPCM, clockwise counter twisted tape, SiC enhanced NF, finned absorber tube.	Overall energy efficiency of 94.1 %.
[16]-2023	Experimental	NPCM, SiC enhanced NF, and twisted absorber tube.	Total energy efficiency of 95.5 %.
[41]-2023	Experimental	Helical tube, nano-emulsions PCM.	Overall energy efficiency of 89.23 %.
[19]-2024	Experimental	Semicircle shape tube, NPCM, and Al_2O_3 enhanced NF.	Total energy efficiency of 91.83 %.
[14]-2024	Numerical	Absorber tubes with serpentine configurations and SiC enhanced NF.	Overall energy efficiency of 60.5 %.
[42]-2024	Experimental and numerical	Absorber tubes with serpentine configurations, PCM, and Copper Foam Matrix (CFM).	Total energy efficiency of 86.48 %.
[43]-2024	Experimental	PCM, absorber tube, Multi-Walled Carbon Nanotubes based NF.	Overall energy efficiency of 76.5 %.
Current study	Experimental	Ribs and Patel array absorber tube, NPCM, SiC enhanced NF, and coiled twisted tapes.	Total energy efficiency of 97.7 %.

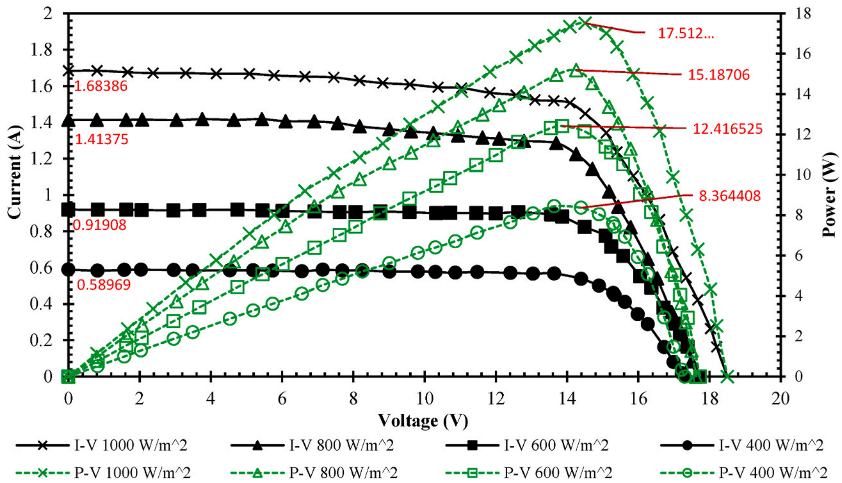

Fig. 10. The I-V and P-V characteristics of the solar cell for The PV alone.

as solar irradiance goes up from 400 W/m^2 to 600, 800, and 1000 W/m^2, the total exergy of the system increases from 9.5 %, which is the total exergy of the system at solar irradiance of 400 W/m^2, to 11.28 %, 12.83 %, and 13.56 %, respectively.

Additionally, employing different cooling techniques, namely 0.3 % SiC enhanced, 0.6 % SiC enhanced, and NPCM increase total exergy efficiency from 13.56 %, which is the total exergy of water at solar irradiance of 1000 W/m^2, and mass flow rate of 0.01 kg/s, to 13.91.7 %, 14.4 %, 15.3 %. The highest total exergy efficiency of 15.3 % is recorded when the mass flow rate of 0.01 kg/s, solar irradiances of 1000 W/m^2, and 0.6%SiC enhanced NF and NPCM are employed. The logarithm of outlet temperature over inlet temperature increases when the mass flow rate is low and solar irradiances are high. At lower mass flow rates, the fluid spends more time in the PVT, causing the outlet temperature to be significantly higher than the inlet temperature. Also, at higher solar irradiances, more heat is transferred to the fluid while it passes through the tubes, causing a more significant outlet temperature to be produced.

After meticulously analysing the effects of different mass flow rates, solar irradiance levels, and coolant types on the overall energy and exergy efficiency of the systems, Table 6 contextualizes the findings by comparing them with results from recent studies that address similar scenarios.

3.5. The I-V and P-V characteristics of the solar cell

As demonstrated in Figs. 10 and 11 which are I-V and P-V graphs of PV alone, PVT with water, SiC enhanced NF, and PVT with NPCM, the maximum power production is always recorded at a mass flow rate of 0.085 kg/s and solar irradiance of 1000 W/m^2. Moreover, employing 0.6%SiC enhanced NF and NPCM offered the best power production. The preceding sections have provided a detailed explanation of why such parameters have recorded the best efficiencies. The power production of the PV alone increases from 8.36 W to 17.512 W as solar irradiance goes up from 400 to 1000 W/m^2. However, as water is employed, it rises to about 24.9 W. Subsequently, it increases to 25.02 W and 25.2 W as 0.3 % and 0.6 % SiC enhanced NF are employed. Finally, it reaches 26 W when

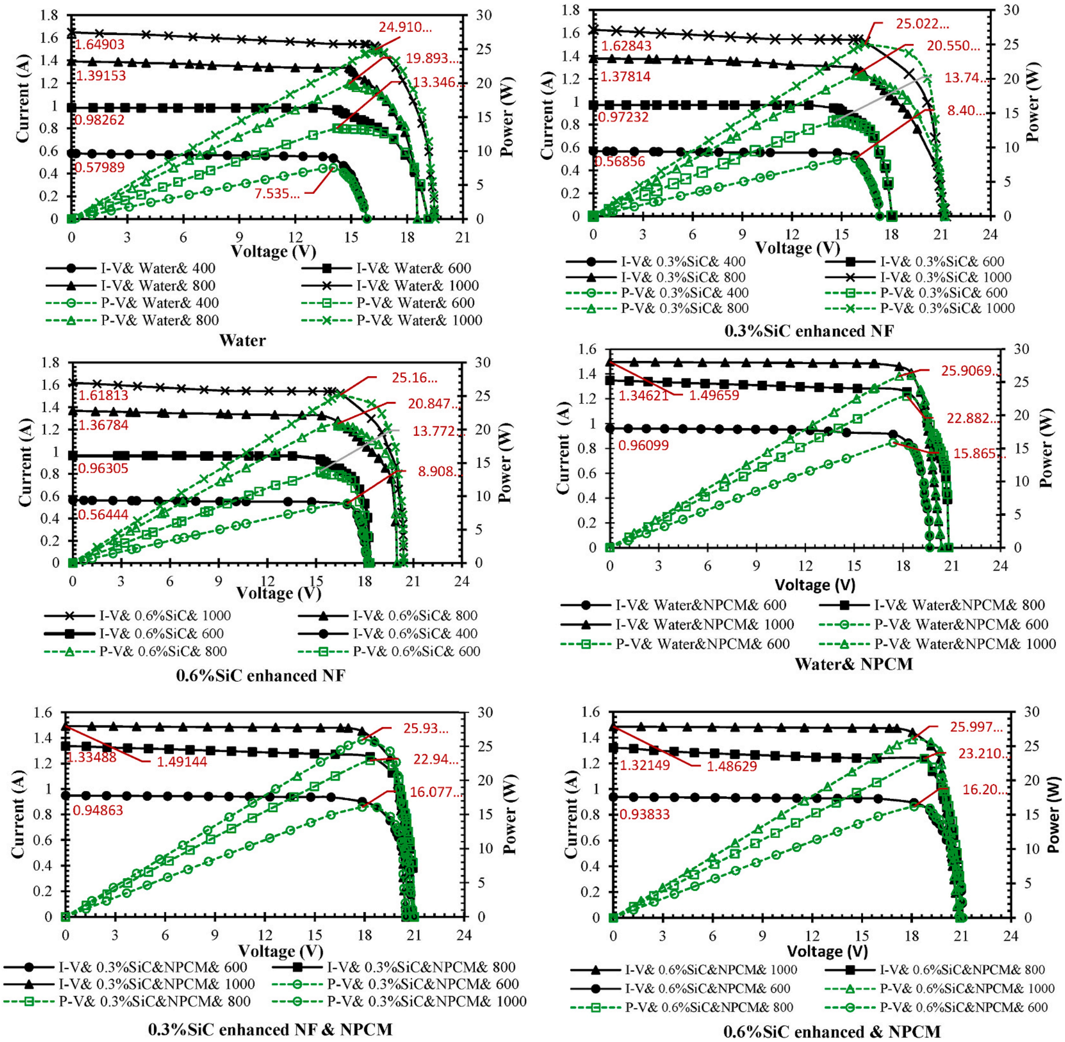

Fig. 11. I-V and P-V characteristics of the PVT for water, 0.3 % and 0.6 % SiC enhanced NF, and NPCM cases.

0.6%SiC enhanced NF and NPCM are incorporated. As additional cooling techniques are applied such as water, 0.3 % SiC enhanced NF, 0.6%SiC enhanced NF, and NPCM for the same mass flow rate and solar irradiance, the solar panel's surface temperature encounters decline, leading to a decrease in short circuit current and maximum current while open circuit voltage, maximum voltage, and maximum power experienced increases. For instance, at a mass flow rate of 0.085 kg/s and solar irradiance of 1000 W/m^2, the short circuit current decreased from 1.6838, which is the value for PV alone, to 1.6490, 1.6284, 1.6181, and 1.4862 A, which are the values for water, 0.3%SiC enhanced NF, 0.6%SiC enhanced NF, and 0.6%SiC enhanced NF & NPCM, respectively. Additionally, maximum power increased from 17.512, which is the maximum power of the PV alone, to 24.9, 25, 25.2, and 26 W, which are the maximum powers for water, 0.3%SiC enhanced NF, 0.6 % SiC enhanced NF, and 0.6 % SiC enhanced NF & NPCM, respectively.

4. Conclusion

The study performs an energy and exergy analysis of a ribbed and petaled array absorber tube equipped with a coiled twisted tape. The study employs SiC enhanced nanofluid and SiC enhanced PCM to improve the PVT's overall efficiency further. Conducting the experiment indoors under mass flow rates of (0.1, 0.025, 0.4, 0.55, 0.7, 0.85) kg/s, solar irradiances of 400, 600, 800, and 1000 W/m^2, and employing water, 0.3 % and 0.6 % SiC enhanced nanofluid, water and nanophase changing materials, and 0.3 % and 0.6 % SiC enhanced nanofluid and nanophase changing materials, the following results were obtained.

- Optimization analysis demonstrates the superior thermal performance of the selected absorber tube over other studied absorber tubes.

- The relationship between mass flow rate and electrical energy and exergy was directly proportional with an impact of a 1–4 % increase.
- The system faces energy and exergy efficiency decline at solar irradiance of 1000 W/m^2 due to lack of sufficient cooling capacity.
- The study's maximum electrical energy and thermal energy efficiencies of the developed design reached 11.2 % and 86.2, respectively.
- The study recorded maximum electrical and total exergy of 11.3 % and 15.3 %, respectively.
- The maximum power of 26 W was recorded in the system.
- The tube featuring ribs and petal arrays equipped with a coiled twisted tape, employing a nanofluid of 0.6 % enhanced nanofluid and nanophase changing material, offered the best cooling capacity.
- As water, 0.3 % SiC enhanced nanofluid, 0.6 % SiC enhanced nanofluid, and nanophase changing materials were applied, the short circuit current and maximum current decreased while voltage and power encountered increased for the same mass flow rate and solar irradiances. In the best-case seniors, the short current decreased from 1.6838, which is for PV alone, to 1.6490, 1. 6284, 1.6181, and 1.4862 A which are the results of water, 0.3 % SiC enhanced nanofluid, 0.6 % SiC enhanced nanofluid, and 0.6 % SiC enhanced nanofluid & nanophase changing material while maximum power output went up from 17.512 to 24.9, 25, 25.2, and 26 W.

Obtaining all the results listed above, the following issues should be addressed in the future research endeavours.

- Conducing a comprehensive Thermohydraulic Performance Factor analysis of the system to shin lights on the heat transfer characteristics of the new design
- Performing outdoor experiment to see the real performance of the new design under real world weather condition.
- Employing more robust passive cooling techniques so that the system's overall performance does not decline at high solar irradiance.

CRediT authorship contribution statement

Banw Omer Ahmed: Writing – original draft, Methodology, Formal analysis, Conceptualization. **Adnan Ibrahim:** Supervision, Methodology, Funding acquisition, Conceptualization. **Hariam Luqman Azeez:** Writing – original draft, Methodology, Formal analysis, Conceptualization. **Sharul Sham Dol:** Writing – review & editing, Supervision, Methodology. **Ali H.A. Al-Waeli:** Validation, Formal analysis. **Mahmoud Jaber:** Writing – review & editing, Validation, Formal analysis.

Declaration of competing interest

The authors declare that they have no known competing financial interests or personal relationships that could have appeared to influence the work reported in this paper.

Data availability

Data will be made available on request.

References

[1] I.O. Harmailil, S.M. Sultan, C.P. Tso, A. Fudholi, M. Mohammad, A. Ibrahim, The state of the art of photovoltaic module cooling techniques and performance assessment methods, Symmetry 16 (4) (2024) 412.
[2] A.A. Abdalkarem, A. Fazlizan, W.K. Muzammil, C.H. Lim, A. Ibrahim, K.H. Wong, H.A. Kazem, The effect of various wedge flap configurations on the performance of wind turbine airfoil, Iranian J. Sci. Techno. Transa. Mech. Eng. (2024) 1–21.
[3] M.A.A.B. Ishak, A. Ibrahim, M.F. Fauzan, A. Fazlizan, W.E. Ewe, H.A. Kazem, The effect of a reversed circular jet impingement on a bifacial module PVT collector energy performance, Case Stud. Therm. Eng. 52 (2023) 103752.
[4] S.M. Sultan, C.P. Tso, K. Sopian, R.K. Ajeel, K. Sobayel, A. Ibrahim, M.Z. Abdullah, Development of assessment methods for photovoltaic module enhancing techniques using the lifespan parameter, Heliyon 9 (11) (2023) e21294.
[5] A.A. Abdalkarem, R. Ansaf, W.K. Muzammil, A. Ibrahim, Z. Harun, A. Fazlizan, Preliminary assessment of the NACA0021 trailing edge wedge for wind turbine application, Heliyon 9 (11) (2023) e21193.
[6] M.A.A.B. Ishak, A. Ibrahim, A. Fazlizan, M.F. Fauzan, K. Sopian, A.A. Rahmat, Exergy performance of a reversed circular flow jet impingement bifacial photovoltaic thermal (PVT) solar collector, Case Stud. Therm. Eng. 49 (2023) 103322.
[7] N.J. Yusaidi, M.F. Fauzan, A. Ibrahim, H. Jarimi, A. Fazlizan, K. Sopian, Recent development on double pass solar thermal collector, Renew. Sustain. Energy Rev. 183 (2023) 113545.
[8] W.E. Ewe, K. Sopian, M. Mohanraj, A. Fudholi, N. Asim, A. Ibrahim, Exergetic performance of jet impingement bifacial photovoltaic-thermal solar air collector with different packing factors and jet distributions, Heat Tran. Eng. (2023) 1–11.
[9] F. Nawab, A.S. Abd Hamid, A. Ibrahim, K. Sopian, A. Fazlizan, M.F. Fauzan, Solar irradiation prediction using empirical and artificial intelligence methods: a comparative review, Heliyon 9, no. 6 (2023) e17038.
[10] J. Assadeg, K. Sopian, A. Ibrahim, A. Fudholi, A.H. Alwaeli, A.S. Abd Hamid, Thermal and thermo-hydraulic performance of finned double-pass solar air collector utilizing cylindrical capsules nano-enhanced PCM, Int. J. Renew. Energy Resour. 13 (1) (2023) 125–135.
[11] F. Nawab, A. Ibrahim, S.Z. Suheel, A.A. Goje, Comparison of ANN global horizontal irradiation predictions with satellite global horizontal irradiation using statistical evaluation, in: 2023 4th International Conference on Computing, Mathematics and Engineering Technologies (iCoMET), IEEE, 2023, March, pp. 1–5.

[12] W.N.A.W. Roshdan, H. Jarimi, A. Ibrahim, K. Sopian, A.H. Al-Waeli, Indoor performance analysis of a novel double-pass photovoltaic/thermal (PV/T) asymmetric compound parabolic concentrator (ACPC) solar collector, in: IOP Conference Series: Materials Science and Engineering, IOP Publishing, 2023, February 012009. Vol. 1278, No. 1.

[13] M.F. Ramlee, A. Ibrahim, H. Jarimi, N. Ramlee, A. Fazlizan, Numerical evaluation of thermal performance of two-phased closed thermosyphon for solar applications, in: IOP Conference Series: Materials Science and Engineering, IOP Publishing, 2023, February 012008. Vol. 1278, No. 1.

[14] N. Jabeen, H.A. Haider, A. Waqas, M. Ali, An effective parametric sensitivity analysis to improve electrical and thermal energy/exergy efficiency of PVT system using nanofluid, Process Saf. Environ. Protect. 189 (2024) 1037–1051.

[15] O. Büyükalaca, H.M. Kılıç, U. Olmuş, Y.E. Güzelel, K.N. Çerçi, Numerical investigation and ANN modeling of performance for hexagonal boron Nitride-water nanofluid PVT collectors, Therm. Sci. Eng. Prog. 43 (2023) 101997.

[16] A.B. Al-Aasam, A. Ibrahim, K. Sopian, B. Abdulsahib, M. Dayer, Nanofluid-based photovoltaic thermal solar collector with nanoparticle-enhanced phase change material (Nano-PCM) and twisted absorber tubes, Case Stud. Therm. Eng. 49 (2023) 103299.

[17] A.M. Bassam, K. Sopian, A. Ibrahim, A.B. Al-Aasam, M. Dayer, Experimental analysis of photovoltaic thermal collector (PVT) with nano PCM and micro-fins tube counterclockwise twisted tape nanofluid, Case Stud. Therm. Eng. 45 (2023) 102883.

[18] M.S. Aziz, A. Ibrahim, M.A.A.B. Ishak, A.B. Al-Aasam, A. Fazlizan, A.S. Abd Hamid, Performance comparison of the standard photovoltaic thermal collector (PVT) and photovoltaic thermal collector with phase change materials (PVT-PCM), Int. J. Renew. Energy Resour. 13 (4) (2023) 1547–1555.

[19] M.M. Maseer, F.B. Ismail, H.A. Kazem, D.M. Hachim, K.A.H. Al-Gburi, M.T. Chaichan, Performance enhancement of photovoltaic/thermal collector semicircle absorber tubes using nanofluid and NPCM, Renew. Energy 233 (2024) 121152.

[20] Z.H. Low, Z. Qin, F. Duan, A review of fin application for latent heat thermal energy storage enhancement, J. Energy Storage 85 (2024) 111157.

[21] Y.M. Ko, J.Y. Song, J.W. Lee, S. Sohn, C.H. Song, M. Khoshvaght-Aliabadi, Y.T. Kang, A critical review on Colburn j-factor and f-factor and energy performance analysis for finned tube heat exchangers, Energy 287 (2024) 129609.

[22] M.W. Aljibory, F.L. Rashid, S.M.A. Alais, An Experimental and numerical investigation of heat transfer enhancement using annular ribs in a tube, in: IOP Conference Series: Materials Science and Engineering, IOP Publishing, 2018, November 012057. Vol. 433, No. 1.

[23] X.W. Li, J.A. Meng, Z.Y. Guo, Turbulent flow and heat transfer in discrete double inclined ribs tube, Int. J. Heat Mass Tran. 52 (3–4) (2009) 962–970.

[24] M.J. Hasan, A.A. Bhuiyan, Thermo-hydrodynamic characteristics and entropy generation in a tube heat exchanger using multiple head ribbed geometries, S. Afr. J. Chem. Eng. 45 (2023) 305–314.

[25] S.K. Sarangi, D.P. Mishra, A comprehensive review on vortex generator supported heat transfer augmentation techniques in heat exchangers, J. Therm. Anal. Calorim. (2024) 1–29.

[26] S. Eiamsa-Ard, P. Promvonge, Performance assessment in a heat exchanger tube with alternate clockwise and counter-clockwise twisted-tape inserts, Int. J. Heat Mass Tran. 53 (7–8) (2010) 1364–1372.

[27] H. Bas, V. Ozceyhan, Heat transfer enhancement in a tube with twisted tape inserts placed separately from the tube wall, Exp. Therm. Fluid Sci. 41 (2012) 51.

[28] P. Promvonge, Thermal augmentation in circular tube with twisted tape and wire coil turbulators, Energy Convers. Manag. 49 (11) (2008) 2949–2955.

[29] H.L. Azeez, A. Ibrahim, B.O. Ahmed, A.H. Al-Waeli, M. Jaber, M.A.A. Rahmat, Energy and exergy analysis of a novel collector design in a photovoltaic thermal system: an experimental study, Appl. Therm. Eng. 256 (2024) 124125.

[30] M.A. Rahman, S.M. Hasnain, S. Pandey, A. Tapalova, N. Akylbekov, R. Zairov, Review on nanofluids: preparation, properties, stability, and thermal performance augmentation in heat transfer applications, ACS Omega 9 (30) (2024) 32328–32349.

[31] B. Singh, S. Sood, Hybrid nanofluids preparation, thermo-physical properties, and applications: a Review, Hybrid Adv. (2024) 100192.

[32] V.T. Rao, Y.R. Sekhar, M. Arıcı, N.R. Pochont, D.R. Prasad, Experimental investigations on bi-symmetrical web flow water based photovoltaic-thermal (PVT) system: energy, exergy, and entropy (3-E) analysis, Sol. Energy 271 (2024) 112445.

[33] M.G. Kibria, M.S. Mohtasim, U.K. Paul, B.K. Das, R. Saidur, Impact of hybrid nano PCM (paraffin wax with Al2O3 and ZnO nanoparticles) on photovoltaic thermal system: energy, exergy, exergoeconomic and enviroeconomic analysis, J. Clean. Prod. 436 (2024) 140577.

[34] A. Alkhalidi, T. Salameh, A. Al Makky, Experimental investigation thermal and exergy efficiency of photovoltaic/thermal system, Renew. Energy 222 (2024) 119897.

[35] M. Ahmadinejad, R. Moosavi, Energy and exergy evaluation of a baffled-nanofluid-based photovoltaic thermal system (PVT), Int. J. Heat Mass Tran. 203 (2023) 123775.

[36] Y. Si, F. Brumercik, C. Yang, A. Glowacz, Z. Ma, P. Siarry, Z. Li, Prediction and evaluation of energy and exergy efficiencies of a nanofluid-based photovoltaic-thermal system with a needle finned serpentine channel using random forest machine learning approach, Eng. Anal. Bound. Elem. 151 (2023) 328–343.

[37] D. De Luca, A. Caldarelli, E. Gaudino, E. Di Gennaro, M. Musto, R. Russo, Modeling of energy and exergy efficiencies in high vacuum flat plate photovoltaic–thermal (PV–T) collectors, Energy Rep. 9 (2023) 1044–1055.

[38] M. Ahmadinejad, A. Soleimani, A. Gerami, Performance enhancement of a photovoltaic thermal (PVT) system with sinusoidal fins: a quasi-transient energy-exergy analysis, Int. J. Green Energy 20 (9) (2023) 978–996.

[39] K.B. Prakash, M.K. Pasupathi, S. Chinnasamy, S. Saravanakumar, M. Palaniappan, A. Alasiri, M. Chandrasekaran, Energy and exergy enhancement study on PV systems with phase change material, Sustainability 15 (4) (2023) 3627.

[40] F. Selimefendigil, D. Okulu, H.F. Oztop, Energy and exergy performance improvement of coupled PV–TEG module by using different shaped nano-enhanced cooling channels, Renew. Energy 234 (2024) 121059.

[41] L. Liu, J. Niu, J.Y. Wu, Improving energy efficiency of photovoltaic/thermal systems by cooling with PCM nano-emulsions: an indoor experimental study, Renew. Energy 203 (2023) 568–582.

[42] M. Dayer, M.A. Shahid, K. Sopian, H.A. Kazem, A.B. Al-Aasam, B. Abdulsahib, A.H. Al-Waeli, Experimental and numerical assessments of a photovoltaic thermal collector equipped with newly configured cooling methods using PCM/CFM, Sol. Energy 276 (2024) 112659.

[43] K. Liu, N. Wang, Y. Pan, T.A. Alahmadi, S.A. Alharbi, G.K. Jhanani, K. Brindhadevi, Photovoltaic thermal system with phase changing materials and MWCNT nanofluids for high thermal efficiency and hydrogen production, Fuel 355 (2024) 129457.